Int J Fract (2017) 208:269–285
https://doi.org/10.1007/s10704-017-0252-9

IUTAM BALTIMORE

Effective simulation of the mechanics of longitudinal tensile failure of unidirectional polymer composites

Rodrigo P. Tavares · Fermin Otero · Albert Turon · Pedro P. Camanho

Received: 22 March 2017 / Accepted: 9 November 2017 / Published online: 22 November 2017
© Springer Science+Business Media B.V., part of Springer Nature 2017

Abstract An efficient computational model to simulate tensile failure of both hybrid and non-hybrid composite materials is proposed. This model is based on the spring element model, which is extended to a random 2D fibre packing. The proposed model is used to study the local stress fields around a broken fibre as well as the failure process in composite materials. The influence of fibre strength distributions and matrix properties on this process is also analysed. A detailed analysis of the fracture process and cluster development is performed and the results are compared with experimental results from the literature.

Keywords Composites · Fracture · Strength · Numerical modelling

1 Introduction

Modelling the longitudinal tensile failure of unidirectional (UD) composite materials is a challenging task due to the complex mechanisms that govern this type of failure. As the main load carrying component, the fibres play an important role in the failure process. It is understood that fibre strength is a stochastic property that is dominated by a distribution of flaws (Argon 1974; Lamon 2007), therefore an accurate characterization of the random nature of fibre strength is necessary to develop proper composite models.

Another important factor in the failure process is the stress redistribution once a fibre is broken and the interaction between multiple fractures leading to the formation of clusters of broken fibres (Pimenta 2015; Scott et al. 2011; Swolfs et al. 2015b; Thionnet et al. 2014). If a cluster reaches a critical size it propagates unstably and causes the failure of the material. When a fibre breaks it does not fully lose its load carrying capability because the surrounding matrix is loaded in shear and transfers stress back onto the unbroken fibre part (Fukuda 1985; Hedgepeth and Van Dyke 1967; Landis and McMeeking 1999; Swolfs et al. 2013a). A region along the fibre called ineffective length is created. In this region the fibre's load carrying capability is hampered, however, at a certain distance away from the breakage the fibre stress carrying capability is fully recovered. The well known Cox's shear-lag model can be used to estimate the ineffective length and stress distribution around the broken fibre (Cox 2002). However, shear yielding of the matrix at the tip of broken fibre will be initiated due to an intensive stress concentration state. To consider this phenomenon, Kelly and Tyson

R. P. Tavares · P. P. Camanho
DEMec, Faculdade de Engenharia, Universidade do Porto, Rua Dr. Roberto Frias, 4200-465 Porto, Portugal

R. P. Tavares · A. Turon
AMADE, Polytechnic School, University of Girona, Campus Montilivi s/n, 17071 Girona, Spain

R. P. Tavares · F. Otero · P. P. Camanho (✉)
INEGI, Rua Dr. Roberto Frias, 400, 4200-465 Porto, Portugal
e-mail: pcamanho@fe.up.pt

(1965) proposed modelling the matrix behaviour within the ineffective length with a perfect-plasticity model, therefore, the ineffective length is calculated from the load balance between the fibre and matrix. Following this ideas, the Global Load Sharing (GLS) model was proposed by Curtin (1991). In this approach, the stress released from a broken fibre is equally distributed among the remaining unbroken fibres. GLS models do not take into account the interaction between the fibres and no local fields due to fibre fracture are considered. Local Load Sharing (LLS) models were developed to take into account fibre interaction in the longitudinal failure of UD composites (Zweben 1968). Several analytical models to determine the stress concentration factor around a single broken fibre (Hedgepeth and Dyke 1967) or in the presence of multiple broken fibres (Batdorf and Ghaffarian 1982; Batdorf 1982; Harlow and Phoenix 1978) have been proposed. In addition, 3D Finite Element Models (3D FEM) have been used to fully model the microstructure of the composite (Mishnaevsky and Brøndsted 2009; Tavares et al. 2016; Xia and Curtin 2001). These models are computationally expensive due to the refined meshes involved and the complex material models required, imposing a limitation in the number of fibres represented in the Representative Volume Element (RVE).

The Spring Element Model (SEM) was proposed by Okabe and co-workers as a low computational cost alternative to 3D FEM (Okabe et al. 2005, 2007). The SEM takes into account local stress redistribution due to fibre failure. The model is based on the assembly of periodic packages of fibre and matrix spring elements. The periodic package or unit cell consists of one fibre surrounded by six other fibres connected through shear spring elements that represent the matrix behaviour. Therefore, the unit cell consists of fibre axial springs in the longitudinal direction and matrix shear springs in transverse direction. This modelling approach has the advantage of being computationally efficient, allowing the simulation of RVEs with a large number of fibres, while allowing to accurately capture the stress redistribution and fibre break interaction during the failure process of UD composites.

The objective of this work is to present a simple, yet accurate and computationally efficient model to predict the failure behaviour of composites using a random fibre distribution. The model should be able to capture the clustering process leading to the ultimate failure of UD composites. The influence of different material properties on the stress redistribution and the failure process zone of composites is analysed in detail.

2 Spring element model for random distribution of different fibres

The model proposed in this section is an extension of the SEM approach to both random distribution of fibres and hybrid composites, where the fibres can have different geometrical and mechanical properties. The SEM consists of longitudinal spring elements, which represent the fibres, connected by transverse spring elements representing the matrix. The matrix contribution in the axial load, i.e. fibre direction, is disregarded in SEM, a commonly accepted hypothesis for UD polymer composites. Therefore, only the matrix shear contribution is represented through shear transverse elements. The stiffness matrices $\mathbf{K}$ of longitudinal and transverse spring elements, from fibre and matrix elements, are given by (Okabe et al. 2005):

$$\mathbf{K}_f = A_f \int_0^l \mathbf{B}_f^T E \mathbf{B}_f dz, \tag{1}$$

$$\mathbf{K}_m = A_m \int_0^d \mathbf{B}_m^T G \mathbf{B}_m dr, \tag{2}$$

where subscripts f and m denote fibre and matrix elements, E is Young's modulus of the fibre, G is the shear modulus of the matrix, $\mathbf{B}$ is the strain-displacement transformation matrix, A_f is the fibre cross section area, A_m is the associated area on the fibre surface of the matrix, l is the fibre's length and d is the distance between surfaces of two adjacent fibres.

2.1 Micro-structure generation and finite element discretization

To obtain the geometric model necessary to represent the composite's micro-structure, a periodic 3D RVE is generated with a random fibre distribution, using the random generator developed by Melro et al. (2008) with the necessary modifications. To guarantee that the RVE has a defined quadrangular geometry, the fibres that are divided by the boundary of the RVE are forced to have its centre at the edge, while ensuring geometric periodicity. With the centre of the fibres defined, ensuring the correct fibre volume fraction and that no fibre overlap occurs, a 2D Delaunay triangulation (Delaunay 1934)

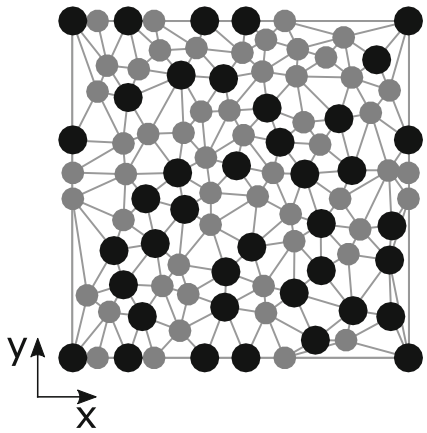

Fig. 1 2D mesh for a periodic RVE with a random fibre distribution

algorithm is used to generate a 2D triangular mesh. Figure 1 shows an example of a mesh, where each circle represents a fibre and each line a matrix shear element. Finally, to generate the 3D RVE mesh the previously obtained 2D mesh is replicated with an offset distance of l^z, which is the predetermined length for fibre spring elements, until the final total desired length of the RVE in fibre direction is achieved. The generated sections are connected through longitudinal fibre spring elements.

Taking $\mathbf{B}_f = \left[1/l^z \ -1/l^z\right]$ and considering that the cross section area of the fibre does not change along the spring element, Eq. (1) can be used to obtain the stiffness matrix for the fibre elements:

$$\mathbf{K}_f^e = \frac{A_f^e E^e}{l^z} \begin{bmatrix} 1 & -1 \\ -1 & 1 \end{bmatrix}, \tag{3}$$

where superscript e refers to element properties or parameters, which can be different for the different fibres involved.

Due to the random distribution of the fibres, two major changes occur with respect to the hexagonal packing used in the original SEM: firstly the distance between each fibre element differs and secondly not all fibre elements are connected to other six fibres, as in the hexagonal packing. The fibres can be connected to, depending on the fibre arrangement, from to three to ten fibres. Therefore, the stiffness of the matrix elements change from element to element, being therefore necessary to change the approach to obtain the stiffness matrix of the matrix shear elements.

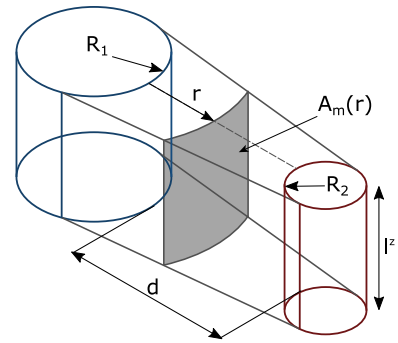

Fig. 2 Matrix shear element connecting 2 fibres

Consider two fibres (1 and 2) with different radii (R_1 and R_2) that are connected to, respectively, n_1 and n_2 fibres, and are separated by a distance d. The associated area on each fibre of the transverse spring element representing the matrix that connects both fibres is, respectively:

$$A_m^{(1)} = \frac{2\pi R_1}{n_1} l^z \quad \text{and} \quad A_m^{(2)} = \frac{2\pi R_2}{n_2} l^z. \tag{4}$$

The area of the matrix element is considered to vary linearly between $A_m^{(1)}$ and $A_m^{(2)}$:

$$A_m(r) = A_m^{(1)} + \frac{\left(A_m^{(2)} - A_m^{(1)}\right)}{d} r. \tag{5}$$

A schematic representation of the fibres and the matrix shear element, which connects both fibres, is shown in Fig. 2.

The shear force on a cross section (at the position r) in the matrix shear element is

$$f_m(r) = G A_m(r) \frac{du}{dr}, \tag{6}$$

where u is the displacement in the longitudinal direction and r is the distance from the fibre 1 surface to the cross section, varying from 0 to d (see Fig. 2). Imposing force equilibrium on a isolated portion of the matrix shear element of radial dimension dr yields:

$$\frac{df_m(r)}{dr} = 0 \quad \Rightarrow \quad \frac{d}{dr}\left(G A_m\,(r)\,\frac{du}{dr}\right) = 0. \tag{7}$$

The solution of Eq. (7) gives the relationship between the shear force on the matrix shear element and the relative displacement of the fibres

$$f_m = \frac{G\left(A_m^{(2)} - A_m^{(1)}\right)}{d \ln\left(A_m^{(2)}/A_m^{(1)}\right)} (u_2 - u_1)\,. \tag{8}$$

Finally, using Eq. (8) the stiffness matrix for the matrix shear element reads:

$$\mathbf{K}_m = \frac{G\left(A_m^{(2)} - A_m^{(1)}\right)}{d \ln\left(A_m^{(2)}/A_m^{(1)}\right)} \begin{bmatrix} 1 & -1 \\ -1 & 1 \end{bmatrix}. \tag{9}$$

The previous matrix equation gives a general expression for the stiffness of a matrix shear element, which will be particularized in each case depending on the connected fibres. For example, the stiffness matrix of the matrix shear element presented in the original SEM (Okabe et al. 2005) is recovered from Eq. (9) by taking the limit when $A_m^{(1)} \to A_m^{(2)}$.

It is interesting to compare the previous result with that obtained using a linear Finite Element to estimate the stiffness matrix of the matrix shear element. Let us consider a node 1 in the fibre 1 and a node 2 in the fibre 2, then the shape functions are:

$$\boldsymbol{\mathcal{N}}_m(r) = \left[\mathcal{N}_1(r)\ \mathcal{N}_2(r)\right] = \left[1 - \tfrac{r}{d} \quad \tfrac{r}{d}\right], \tag{10}$$

and the stiffness matrix is obtained by:

$$\int_0^d \frac{d\boldsymbol{\mathcal{N}}_m}{dr^T} G A_m \frac{d\boldsymbol{\mathcal{N}}_m}{dr} dr, \tag{11}$$

where A_m is given by Eq. (5). Solving Eq. (11) the stiffness matrix of the matrix shear element using a FEM approach is obtained:

$$\tilde{\mathbf{K}}_m = \frac{G\left(A_m^{(2)} + A_m^{(1)}\right)}{2d} \begin{bmatrix} 1 & -1 \\ -1 & 1 \end{bmatrix}. \tag{12}$$

Note that $\tilde{\mathbf{K}}_m$ can be seen as a linearisation of the stiffness matrix $\mathbf{K}_m$ obtained previously around the $A_m^{(1)} \to A_m^{(2)}$ point. If the associated areas ($A_m^{(1)}$ and $A_m^{(2)}$) on each fibre are not substantially different, Eq. (12) represents a good approximation of $\mathbf{K}_m$. In any case, Eq. (9) i.e. $\mathbf{K}_m$, will be used in this work to obtain the stiffness matrix for the matrix shear element.

As previously explained, the 3D RVE is generated by extruding the 2D mesh (see Fig. 1) with fibre elements connecting each of the sections. Therefore, the virtual work of the total spring-element model is

$$\delta\mathbf{u}^T \left[\left(\sum_{e=1}^{N_f - N_f^b} \mathbf{K}_f^e + \sum_{e=1}^{N_m} \mathbf{K}_m^e \right) \mathbf{u} \right] = \delta\mathbf{u}^T \mathbf{f}, \tag{13}$$

where N_f and N_m are the total number of fibre and matrix elements, $\mathbf{u}$ and $\mathbf{f}$ the displacement and force vectors and N_f^b is the number of broken fibre elements, respectively. $\mathbf{K}_f^e$ is given by expression shown in Eq. (3), while $\mathbf{K}_m^e$ is the stiffness matrix of the each individual matrix shear element [(see Eq. (9)]. Finally, the nodal displacements in the proposed modification of the SEM are obtained by solving

$$\mathbf{K}\mathbf{u} = \mathbf{f}, \tag{14}$$

where $\mathbf{K}$ is the global stiffness matrix,

$$\mathbf{K} = \sum_{e=1}^{N_f - N_f^b} \mathbf{K}_f^e + \sum_{e=1}^{N_m} \mathbf{K}_m^e. \tag{15}$$

2.2 Failure modelling

For the fibre elements a failure criteria associated with the longitudinal failure mechanism is considered, which can be written in its general form as

$$\frac{\sigma_f}{X_T^e} - 1 < 0 \quad \text{if} \quad \sigma_f > 0, \tag{16}$$

where σ_f is the fibre stress and X_T^e is the tensile strength of the fibre element. As will be seen in the next section, the tensile strength of an element i.e. X_T^e will be randomly assigned recurring to one of the available statistical distributions to describe fibre's strength. In the present implementation a fibre element will be considered fully damaged if the failure criteria given by Eq. (16) is not satisfied. Therefore, when a fibre element does not verify Eq. (16) it is considered broken and N_f^b updated accordingly.

The matrix behaviour plays an important role in the tensile failure of composite materials, since this is the element that allows stress redistribution to occur after a fibre breaks. This stress-redistribution is affected by both matrix plasticity and damage, as well as fibre-matrix decohesion (Nishikawa et al. 2008; Tavares et al. 2016). The matrix was considered to be linear elastic and perfectly plastic. This behaviour was implemented

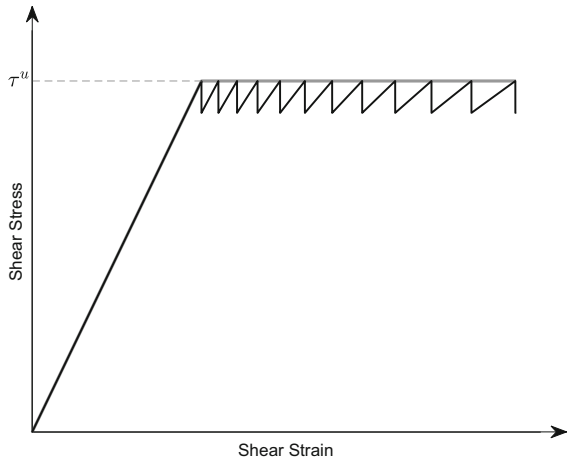

Fig. 3 Saw-shape matrix behaviour using sequentially linear analysis, in black, and analytical behaviour in grey

in the model using sequentially linear analysis (DeJong et al. 2008; Rots and Invernizzi 2004).

The sequentially linear approach approximates the constitutive stress-strain relationship using a series of saw-teeth that maintain a positive tangent stiffness. Linear analyses are repeated, each with a reduced positive stiffness, until the global analysis is complete. Thus, the negative or null tangent stiffness, which is characteristic of softening curves, that can be detrimental to convergence, is entirely avoided.

In a sequentially linear strategy, the stress-strain diagram can be reproduced by a consecutively reducing the shear stiffness (G_i) as well as changing the yield stress of each critical element (τ_i^u). The shear stiffness is reduced in a discrete manner according to:

$$G_{i+1} = \frac{G_i}{\alpha_m} , \tag{17}$$

where α_m is a parameter larger than one and that can be controlled by the user, ensuring a control in accuracy versus computational time. The behaviour of the matrix is dominated by an envelope curve that determines when each stiffness reduction occurs and the new yield stress of the material is defined. In this paper, the behaviour considered is a linear elastic perfectly plastic behaviour, characterized by a constant yield stress (τ^u). Both the accurate and the approximation using the sequentially linear analysis of the matrix behaviour considered are shown in Fig. 3.

Although being used only to simulate elastic and perfect plastic model in this work, this is a versatile implementation that allows the behaviour to the matrix to be changed to consider any type of constitutive behaviour. It should be noted that, while there is a reduction of the stiffness of the matrix elements during the sequentially linear analysis procedure, the number of connections in each fibre (n_1 and n_2) is not changed.

In this model the stresses on the fibre elements in the ineffective length are not imposed, but are obtained from the overall equilibrium of the system together with the failure criterion proposed for the matrix shear elements.

2.3 Numerical implementation

The flowchart of numerical implementation of the model proposed is shown in Fig. 4. The model was

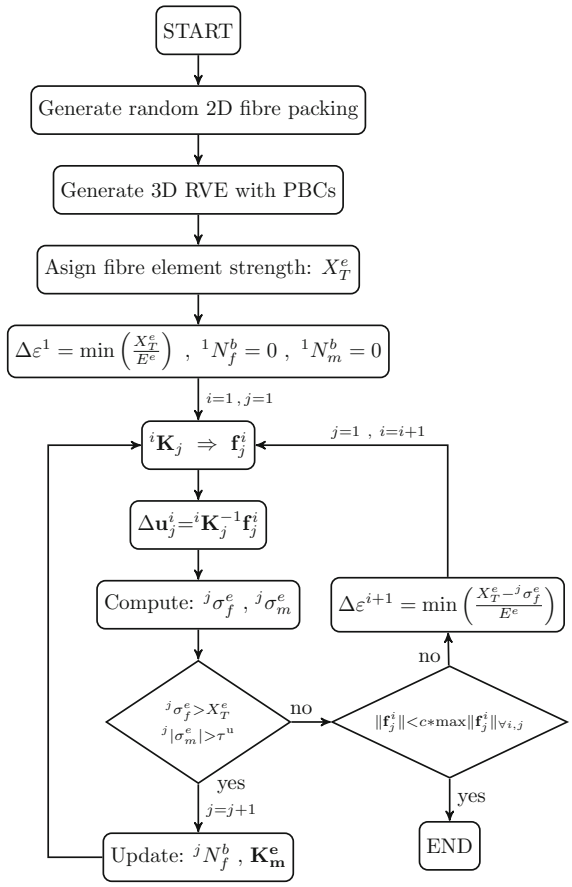

Fig. 4 Flowchart of the the model implemented

implemented using the commercial software MATLAB®.

Firstly, the RVE geometry is generated with a 2D random fibre distribution, which is then extruded to generate the 3D periodic RVE. For all the fibre elements and according to an adequate fibre strength distribution a random strength is assigned to each of the fibre elements.

An evolutive strain incrementation procedure is considered to ensure that a strain increment only forces one fibre to fail, given generally by:

$$\Delta\varepsilon = \min\left(\frac{X_T^e - \sigma_f^e}{E^e}\right), \tag{18}$$

where σ_f^e is the stress in the fibre element from the previous strain increment. The global stiffness matrix of the model with the updated number of broken fibre elements and updated matrix shear stiffness is determined. Displacement control is considered in the model and the applied displacement is calculated based on the strain increment given in Eq. (18) and the RVE dimension. The external force vector f_j^i is obtained based on the current stiffness matrix and the applied displacement. Solving the system of equations (14) the unknown displacement vector is calculated. From the displacement vector the strains and stresses in all the elements are determined. Periodic Boundary Conditions (PBCs) (Otero et al. 2015) are considered when solving the system of equations, which is possible due to the material periodicity of the RVE. The implementation of the PBCs is done through the elimination of the redundant degrees of freedom on the RVE boundary.

A failure criteria for the fibres as well as a elastic and perfectly plastic model for the matrix were implemented. If any of the fibre elements fail or if the shear stress in the matrix elements exceeds τ_i^u, the number of broken fibre elements is updated as well as the stiffness of the matrix elements. Then a new global stiffness matrix is computed and the system of equations is solved once more. This iterative process continues until no fibre or matrix element fail and equilibrium has been achieved. If equilibrium is achieved and the termination criterion is not met, a new strain increment is determined and the iterative process continues. If the termination criterion is met, then the simulation finishes. The termination criterion used stops the algorithm once the norm of the external force vector in the current iteration is lower than c times the maximum norm of the external force vector from all the previous increments, where c is a value between zero and one. The numerical results shown in this work are obtained using a value of c equal to 0.2.

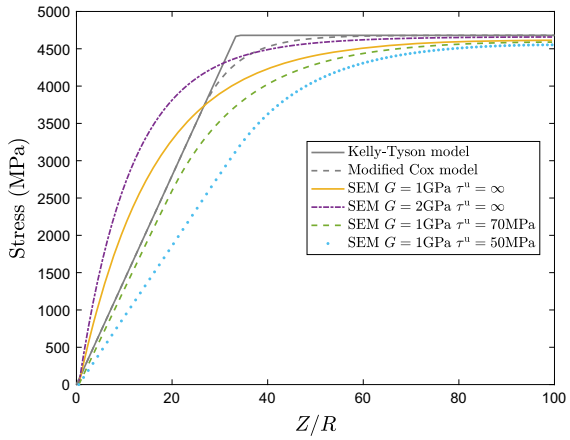

Fig. 5 Influence of matrix properties on the stress recovery profile of a broken fibre

3 Mechanisms of longitudinal failure

3.1 Local fields around a broken fibre

To verify if the model is capable of correctly capturing the stress profile of a broken fibre, several simulations were performed using an RVE with a transverse section of 87.5×87.5 μm composed of 132 fibres with a length of 350 μm. The fibres used for these simulations are the AS4 carbon fibres (Curtin and Takeda 1998), whose properties are: $E_f = 234$ GPa, $R_f = 3.5$ μm.

The ineffective length of a broken fibre in this model is not only controlled by the shear modulus of the matrix (G) but also by the yield stress (τ^{u}). Figure 5 shows the influence of the matrix shear modulus and yield stress in the stress recovery profile of a broken fibre. For comparison purposes the Kelly–Tyson (Kelly and Tyson 1965) and modified Cox (Landis and McMeeking 1999) shear-lag models are shown, using a fibre-matrix interfacial strength of 70 MPa and a matrix shear modulus of 1 GPa. The results shown were obtained considering an applied strain of 2%.

It can be observed in Fig. 5 that the stress recovery profile of a broken fibre is captured by the model, Z

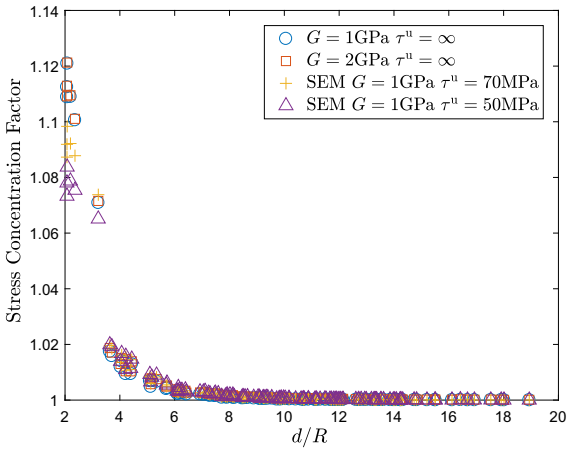

Fig. 6 Stress concentrations as a function of the distance to the broken fibre

is the distance from the break plane in the longitudinal direction. While there are some differences between the stress profile obtained by the SEM and the simplified shear-lag models, the profile is considered to be accurate and therefore there is no need to superimpose the shear-lag profile in the modelling strategy. In this figure, it is also possible to see that limiting the maximum stress in the matrix shear elements affects the recovery profile and therefore the ineffective length, which is increased. This is discussed in more detail at the end of this section.

When a fibre breaks there is not only an ineffective length in the broken fibre, but the stress previously carried by this fibre is redistributed among the surrounding intact fibres, increasing the stress carried by these fibres and thus increasing their failure probability. The increase of stress can be quantified by a Stress Concentration Factor (SCF), considered here to be the ratio of the actual stress in the fibre over the stress in the fibre if there were no breaks, given by $E_f\varepsilon$, where ε is the applied strain. This SCF is affected by the matrix and fibre properties as well as by the fibre arrangement. Figure 6 shows the SCF as a function of the distance between the centre of a given fibre and the centre of the broken fibre (d), in the fracture plane. The results are shown for matrix shear modulus of 1 GPa, with $\tau^u = \infty$, $\tau^u = 70$ MPa and $\tau^u = 50$ MPa and 2 GPa with $\tau^u = \infty$.

The SCF decreases away from the broken fibre, being this decrease continuous if no matrix yield stress is considered, i.e., the matrix is considered linear elastic. If matrix yield stress is considered the stress redistribution is more complex as there is a maximum matrix shear stress in the matrix shear elements, causing the stress redistribution to be less uniform and more dependent on the actual fibre arrangement. To better visualize this stress redistribution the stress concentration factor in each intact fibre that surrounds the broken one is plotted in Figure 7. Figure 7a, b show the predictions for different values of the matrix stiffness, maintaining $\tau^u = \infty$. It is observed that the stress concentrations

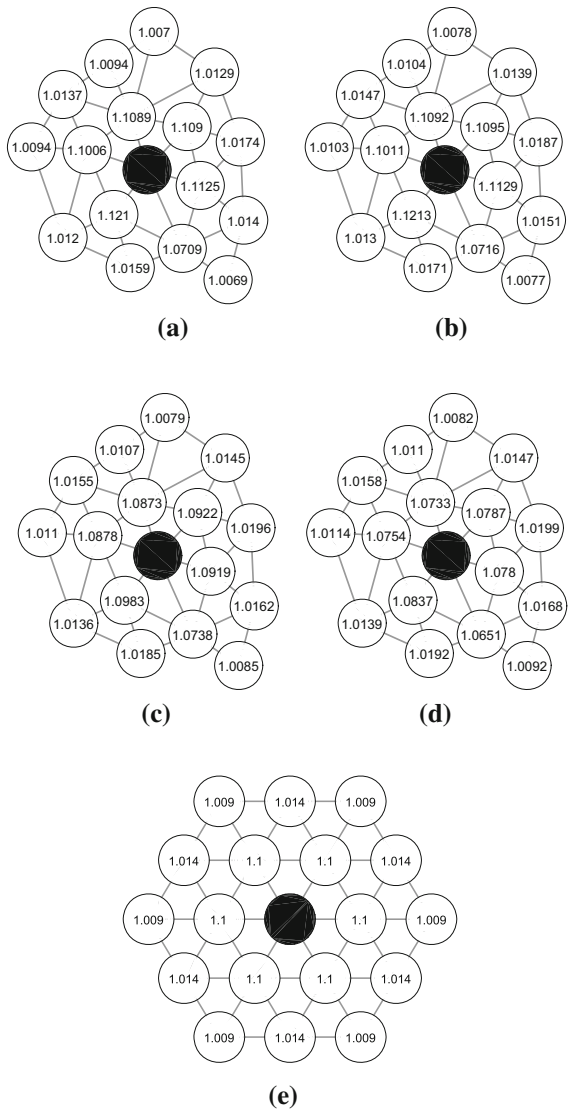

Fig. 7 Stress concentrations in the intact fibre surrounding a broken fibre **a** $G = 1$GPa and $\tau^u = \infty$ **b** $G = 2$GPa and $\tau^u = \infty$ **c** $G = 1$GPa and $\tau^u = 70$MPa **d** $G = 1$GPa and $\tau^u = 50$MPa **e** Hexagonal packing with $G = 1$GPa and $\tau^u = \infty$

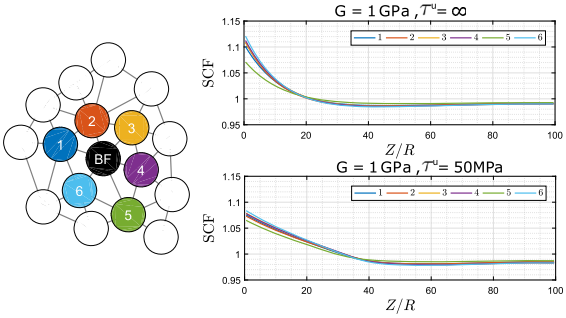

Fig. 8 Stress concentrations in the intact fibres as a function of the distance to the fibre break plane

are higher in the surrounding fibres for the higher shear stiffness of the matrix. When a matrix limit stress is considered the analysis of the stress redistribution becomes more complex (Fig. 7c, d): for the fibres closer to the broken one the SCF is reduced, while for the remaining ones the SCF increases to maintain the equilibrium. Therefore, the in-plane stress recovery region is increased while the maximum SCF is decreased. This stress redistribution is not trivial to predict, not only on the fracture plane but along the broken fibre's ineffective length, being this dependent on the matrix properties as well as on the fibre distribution. Nonetheless, this stress redistribution process is not imposed in the model, as in several available models (Swolfs et al. 2015a), but it is directly obtained from the equilibrium equations. For comparison purposes the stress concentration factors of an hexagonal packing are shown in Fig. 7e, from which is possible to see that the maximum SCF is lower than that obtained using random packing.

As mentioned before, the effect of limiting the maximum shear stress in the matrix elements not only changes the stress concentrations in the plane of the fracture, but also the stress redistribution within the ineffective length. To better understand this redistribution process, the stress along the intact fibres that surround a broken one are shown in Fig. 8, for both the cases with and without matrix yield stress and with $G = 1$ GPa. When no yield stress is considered, it is possible to see that the SCF is maximum in the fracture plane and steadily decreases until the far field stress is reached. The differences in stress concentrations between the intact fibres is a consequence of the fibre arrangement and its effect on the shear stiffness of the matrix elements connecting the broken to each of the intact fibres. When $\tau^u = 50$ MPa is considered, it is possible to see that the shape of the stress profile in the intact fibres changes, being now linear in the regions closer to the broken fibre. This is due to the fact that the matrix elements that connect these fibres to the broken one are within the plastic zone and, therefore, their stress is independent of the applied strain, being equal to 50 MPa. Although the maximum stress concentration is reduced when a yield stress is considered, the intact fibres have an higher SCF away from the break plane, which may increase the failure probability of these fibres. In addition, the in-plane stress recovery region is also increased. In spite of the differences in stress redistribution being small, these effects may be amplified when more than one fibre breaks in a single cluster, being that there are more than one interacting fibre fractures. These differences in stress redistribution may affect the fracture process in composite materials leading to differences in cluster formation.

3.2 Influence of the fibre strength distribution

The tensile failure of composite materials is a fibre dominated process, therefore, it is necessary to accurately capture the fibre's stochastic strengths. Fibres exhibit weakest-link characteristics and their strength is flaw dominated. The most used statistical distribution to describe the strength of the fibres is the Weibull distribution (Weibull 1951):

$$P(\sigma) = 1 - \exp\left(-\left(\frac{L}{L_0}\right)\left(\frac{\sigma}{\sigma_0}\right)^{\rho}\right), \tag{19}$$

where P is the failure probability at the applied stress σ, L is the characteristic gauge length, L_0 is the reference gauge length, σ_0 the scale parameter and ρ the shape parameter or Weibull modulus (Weibull 1951). Although being the most used statistical distribution for fibre strength, it has been shown that the Weibull distribution is not the best suited for carbon and glass fibres (Beyerlein and Phoenix 1996; Curtin 2000; Gulino and Phoenix 1991). To better capture the experimental data different distributions have been proposed, usually based on the Weibull distribution such as the Power-Law Accelerated Weibull (PLAW) (Curtin 2000; Padgett et al. 1995; Watson and Smith 1985):

$$P(\sigma) = 1 - \exp\left(-\left(\frac{L}{L_0}\right)^{\alpha}\left(\frac{\sigma}{\sigma_0}\right)^{\rho}\right), \tag{20}$$

where α is an additional parameter for the distribution. A consequence of this exponent α, which is lower than one, is that for lengths smaller than the reference L_0 the strength distribution shifts to lower strengths. This drastically changes the behaviour of the models, as usually, very small element lengths are considered and if the length scaling is not accurately captured by the statistical distribution, the element's strength can be largely over predicted.

Curtin (2000) proposed another model entitled Weibull of Weibulls (WOW) that conforms with Eq. (20) but with more solid physical background. This model assumes that the strength distribution along a fibre is a Weibull distribution with modulus ρ' and that the characteristic strength of each fibre follows a different Weibull distribution with modulus m. The different characteristic strengths of the fibres are attributed to the processing and handling of the fibres. This distribution yields Eq. (20) if the following relations are met:

$$\rho = \frac{m\rho'}{\left(m^2 + \rho'^2\right)^{1/2}}, \tag{21}$$

and

$$\alpha = \frac{m}{\left(m^2 + \rho'^2\right)^{1/2}}. \tag{22}$$

The difference between the PLAW and WOW models is that, in the WOW model the strength along an individual fibre is highly correlated, leading to very weak and very strong fibres, while in the PLAW model there is no direct correlation in the strength of the elements within a single fibre.

Several simulations using different random distributions were performed using each of the presented strength distributions. The models used have approximately 1100 fibres, with a length of 1.05 mm, divided into 150 elements along its length. The transverse dimension of the RVEs is 260 × 260 μm. AS4 fibres have been considered with the properties shown in Table 1, obtained from Curtin (2000). The fibre volume fraction was considered to be 60%, the shear modulus of the matrix 1 GPa and the matrix elements were considered linear elastic ($\tau^{u} = \infty$). For each distribution, five simulations were performed. For each simulation a new random microstructure was generated as well as know random element strengths. For the WOW strength distribution, five simulations with a periodic hexagonal fibre arrangement was also simulated. A summary of some relevant results of the simulations are shown in Table 2, which include the maximum cluster size that will be defined in Sect. 3.4.

Table 1 AS4 carbon fibre properties (Curtin 2000)

σ_0	4275 MPa
ρ'	10.7
L_0	12.7 mm
ρ	6.4
α	0.6
m	8

Figure 9 shows the results of the simulations performed using all the three strength distributions presented above. The traditional Weibull distribution leads to a higher composite strength prediction when compared with PLAW and WOW distributions. This is due to the large difference between L_0 and $L = l^z$, which leads to a higher individual tensile strength of the fibre elements. Using the PLAW or WOW model leads to lower tensile strengths, as the length scaling is affected also by the α parameter, leading to a reduction of the elements individual tensile strength and, therefore, to a reduction of predicted composite tensile strength.

Madhukar and Drzal (1991) tested AS4 composites in an EPON 828 matrix and obtained a tensile strength for the composite material of 1890 MPa and a failure strain of 1.45% for a measured fibre volume content of 67.7%, however, according to Curtin (2000), the measured Young's modulus is more consistent with an effective volume fraction of 59%, which is consistent with the volume fraction considered in the simulations. From the results shown in Fig. 9, it is observed that the Weibull distribution leads to an overprediction in both tensile strength and failure strain. While, the PLAW and WOW models give better results. The WOW distribution gives the results closer to the experimentally obtained, with an average tensile strength of 1951 MPa and a failure strain of 1.67%. It should be noted that size effects are present in composite materials and the size of the tested coupon and of the RVE are different.

Table 2 and Fig. 9 also show the results from simulations with an hexagonal arrangement of fibres with

Table 2 Maximum stress, failure strain and maximum cluster size for the AS4 composite using different strength distributions and fibre distribution

	Sim.	1	2	3	4	5	Avg.	STDV
Weibull	X_T (MPa)	3365	3436	3370	3369	3366	3381	30.78
	ε_f (%)	2.74	2.82	2.64	2.75	2.64	2.72	0.08
	Max. cluster	23	29	14	28	19	23	6.27
PLAW	X_T (MPa)	2117	2095	2125	2137	2105	2116	16.41
	ε_f (%)	1.71	1.76	1.72	1.73	1.71	1.73	0.02
	Max. cluster	15	33	24	25	23	24	6.40
WOW	X_T (MPa)	1939	1978	1948	1928	1961	1951	19.61
	ε_f (%)	1.65	1.73	1.66	1.68	1.65	1.67	0.03
	Max. cluster	20	27	36	19	16	23	8.02
WOW hexag.	X_T (MPa)	1934	1958	1938	1930	1947	1941	11.21
	ε_f (%)	1.67	1.66	1.61	1.61	1.68	1.65	0.03
	Max. cluster	40	34	20	22	45	32	10.96

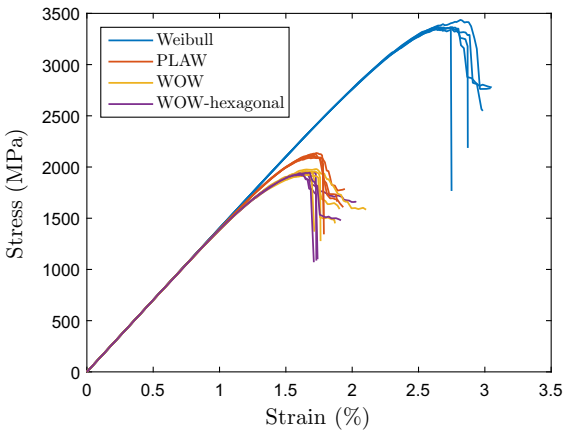

Fig. 9 Stress-strain curves for AS4 non-hybrid composites using different strength distributions

the WOW strength distribution. Comparing the random and hexagonal fibre distributions it is possible to see that the stress-strain behaviour is not affected by the arrangement. An interesting characteristic of the stress-strain curves is that there is a high non-linearity previous to the failure of the material, which is usually not seen in the experimental results. This fact will be analysed in more depth in Sect. 3.4.

3.3 Influence of the matrix properties

As explained in Sect. 2.2 a material model was implemented for the matrix that allows to simulate and elastic-perfect plastic behaviour of the matrix. This has an effect on both stress concentrations and on the ineffective length as shown in Sect. 3.1 and, therefore, should also affect the failure process in a multi-fibre composite.

Figure 10 shows the stress-strain curves for an AS4 composite where the fibre strength is characterized by a WOW distribution, for different yield stresses (τ^{u}), as well as different matrix shear modulus (G). Table 3 shows the main properties of the failure process for these simulations. From the analysis of these simulations it is possible to conclude that limiting the maximum shear stress in the matrix significantly reduces the tensile strength of the composite material, leading to an earlier failure and, therefore, also a lower failure strain. This change in the stress-strain behaviour is also accompanied by a change in the fracture process, being that the maximum cluster size determined was reduced from 23 to 18 and 14 broken fibres, which relates better with the experimental results of Scott et al. (2011) and the modelling results of Swolfs et al. (2015b). This can be explained by the lower maximum SCF as seen in Sect. 3.1 when a yield stress is considered. When comparing the results for both $\tau^{\mathrm{u}} = 50$ MPa and $\tau^{\mathrm{u}} = 70$ MPa it is possible to conclude that the stress-strain behaviour does not change much, leading to very similar tensile strengths, only with a slightly smaller tensile strength and critical cluster size.

The results shown in Fig. 10 and Table 3 enable the study of the influence of changing the matrix shear

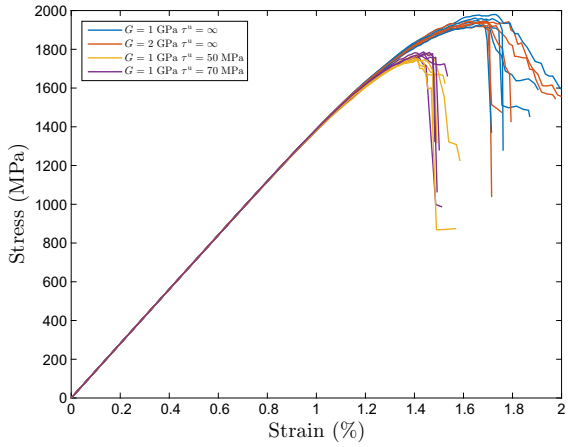

Fig. 10 Stress-strain curves for AS4 non-hybrid composites with different matrix properties

modulus from 1 to 2 GPa. It is possible to conclude that the matrix shear stiffness does not affect the stress-strain behaviour of the composite, leading to similar tensile strengths and failure strains. However, it clearly affects the maximum cluster size, which is increased from 23 to 72 broken fibres. This means that although the stress-strain curves are similar, the failure process is different, with the fibres breaking more closely with the higher matrix shear stiffness, allowing to the formation of larger clusters before the specimen dramatically looses load carrying capability.

3.4 Analysis of cluster formation

The model proposed here can also be used to analyse the development of clusters of broken fibres during the failure process. A cluster is defined following Swolfs et al. (2015b): two fibres are considered to be part of the same cluster if (i) the distance between the centres of the two fibres is lower than four times the fibre radius and (ii) the axial distance between break planes was less than ten times the fibre radius. Swolfs et al. (2015b) defines two type of clusters: disperse clusters if the axial distance between the break planes is higher than a fibre radius and co-planar cluster if this distance is lower. In this work a cluster is considered co-planar if the break planes in the axial direction distance themselves by no more than one axial element length. The maximum cluster size for each simulation using the three different strength distributions is shown in Tables 2. The maximum cluster size does not significantly change with the different strength distributions, being this maximum around 23–24 fibres in average. However, there are simulations where it has gone as high as 36 fibres and as low as 14 fibres, due to the randomness of the element strength assignment. Although the cluster size does not change with the strength distribution it changes when comparing the hexagonal and random fibre packings: the mean maximum cluster size in the hexagonal packing equal to 32 while for the random packing is 23. In Sect. 3.3 it was seen that limiting the shear stress in the matrix elements affects

Table 3 Maximum stress, failure strain and maximum cluster size for the AS4 considering different matrix properties with the WOW strength model and random fibre distribution

	Sim.	1	2	3	4	5	Avg.	STDV
$\tau^u = \infty$ $G = 1$GPa	X_T (MPa)	1939	1978	1948	1928	1961	1951	19.61
	ε_f (%)	1.65	1.73	1.66	1.68	1.65	1.67	0.03
	Max. cluster	20	27	36	19	16	23	8.02
$\tau^u = \infty$ $G = 2$GPa	X_T (MPa)	1941	1918	1946	1945	1937	1937	11.48
	ε_f (%)	1.79	1.65	1.68	1.63	1.64	1.68	0.07
	Max. cluster	135	50	62	49	64	72	35.87
$\tau^u = 70$MPa $G = 1$GPa	X_T (MPa)	1784	1798	1848	1842	1839	1822	29.02
	ε_f (%)	1.41	1.40	1.49	1.50	1.52	1.46	0.06
	Max. cluster	12	12	25	25	18	18	6.50
$\tau^u = 50$MPa $G = 1$GPa	X_T (MPa)	1787	1774	1794	1777	1787	1784	8.22
	ε_f (%)	1.45	1.44	1.44	1.46	1.45	1.45	0.01
	Max. cluster	17	11	21	11	10	14	4.80

not only the stress-strain behaviour but also the cluster formation, being therefore essential to consider this behaviour when analysing cluster formation.

On the previous sections the behaviour of an AS4 composite material was analysed, however, to further analyse the fibre break clustering process and to compare the numerical results and the experimental results by Scott et al. (2011, 2012) the behaviour of the T700 carbon composite material is studied. Following Watanabe et al. (2014) a bimodal Weibull distribution, which assumes that there are two flaw distributions, is used to represent the fibre strength. This distribution is characterized by two Weibull modulus and scale parameters. The parameters used are (Watanabe et al. 2014): $\sigma_{01} = 5200$ MPa, $m_1 = 4.8$, and $\sigma_{02} = 6100$ MPa, $m_2 = 12$ at $L_0 = 10$ mm. The elastic modulus considered was 238 GPa and the fibre radius used was $R_f = 3.5$ μm. The matrix used in the experimental results of Scott et al. (2012) was M21 which has a tensile modulus of 1.26 GPa. Considering Poisson's ratio of 0.4, the matrix shear modulus used was $G = 0.45$ GPa and the matrix yield stress considered was $\tau^u = 50$ MPa. The RVEs used have a fibre volume fraction of 55% and are of equal dimensions has the ones used in the previous sections.

Five simulations were performed and the results were averaged to minimize the effect of the random fibre strength. As the fibre behaviour was considered linear elastic up to failure the failure strain is overpredicted and equal to 2.61%, comparing with the 1.89%, shown in the experimental results. This large difference can be explained by the typical non-linear behaviour of T700 carbon fibres, which for an 1% increase in strain can have a 20% increase in stiffness (Swolfs et al. 2015b; Toyama and Takatsubo 2004). Considering that the material would fail at the same stress level, if the non-linearity was considered, the failure strain would be approximately 2%, which is in better agreement with the experimental result.

The average maximum cluster size before the unstable propagation obtained in the simulations was 12.6 fibres, which is slightly smaller than the 14 observed experimentally Scott et al. (2012). Figure 11 shows the experimental and numerical comparison of the fibre break density. It can be seen that the fibre break density is clearly overpredicted. The very large discrepancy between the two results can be attributed to the inaccuracy of the Weibull distribution. Swolfs et al. (2015b) also attributes this difference to the in situ

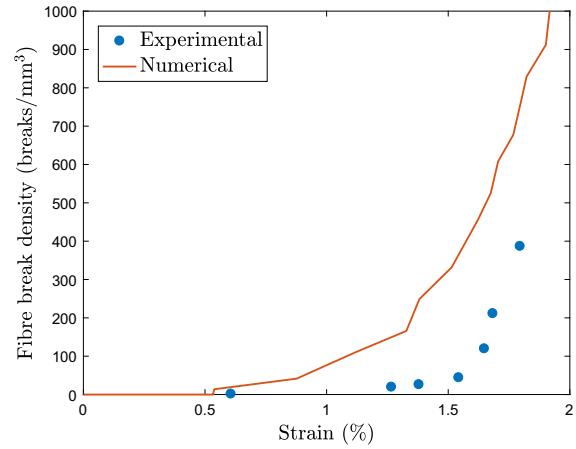

Fig. 11 Fibre break density in the fracture process: experimental and numerical results for bimodal Weibull distribution

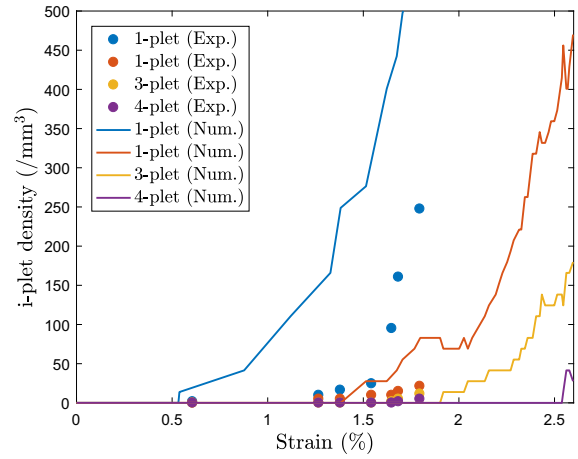

Fig. 12 i-plet growth during the fracture process as a function of the applied strain: experimental and numerical results for bimodal Weibull distribution

defect sensitivity reduction of the fibres when surrounded by matrix, altering therefore the actual strength distribution of the fibres within the composite material. Another discrepancy between the experimental results and the numerical ones is that the fibre break density at failure is much higher in the numerical results. While in the experimental results, before failure, less than 10% of the fibres were broken, in the numerical results this number approximately 30%. These differences in cluster formation process and a higher fibre break density prior to the failure of the material may explain the non-linearity seen in the stress-strain curves prior to failure, which usually are not present in the experimental results.

To better understand the differences in fibre break density between the model and the experimental results the cluster development needs to be analysed in more detail. Figure 12 shows the evolution of clusters of different sizes (i-plets) as a function of the applied strain. From the results it is possible to conclude that the singular fibre breaks (1-plet) occur at lower strains and grow rapidly, which are the main contributors for the higher fibre break density in the numerical results. The clusters of two fibres (2-plet) start appearing at similar strains in the numerical and experimental results, however, the cluster with higher number of fibres (3-plet and 4-plet) appear at higher strains in the numerical results. In the experimental results up to 50% of the breaks occurred in clusters (Swolfs et al. 2015b), however, the model only predicts that 10–20% of the fibre breaks occur in cluster, being the majority of them singular breaks. Additionally only 30–40% of the clusters were co-planar in comparison to a value of 70% found in the experiments. It is interesting to note is that while in the experiments when a cluster was formed it remained of constant size, in the numerical results this was not the case (a cluster increases in size with the applied strain). These results show that there is an under prediction of the SCF in the surrounding fibres when a fibre breaks. Swolfs et al. (2013b) found that the SCFs are increased if a matrix crack surrounding the broken fibre is considered. This is not considered in the model and can be a source of underestimation of the SCFs. Additionally, it has been shown that when a fibre breaks there is a dynamic effect that causes an increase in the SCFs in the intact fibres (Tavares et al. 2016; Xing et al. 1985).

To circumvent some of the issues with the bimodal Weibull distribution used, Swolfs et al. (2015b) fitted an unimodal Weibull distribution to the fibre break density data. A good fit was obtained for $\sigma_0 = 5200$ MPa and $m = 10$ at $L_0 = 10$ mm. Using this distribution and the same matrix properties as in the previous simulations, there was a reduction in the average failure strain to 2.37%, which is closer to the experimental value but still above. This fact may result from the non-linearity of the fibres, but also from the underestimation of the cluster formation. With the fitted Weibull distribution the fibre break density observed numerically is in better agreement with the experimental results (Fig. 13), however, it is still observed that failure occurs at higher failure fibre break densities.

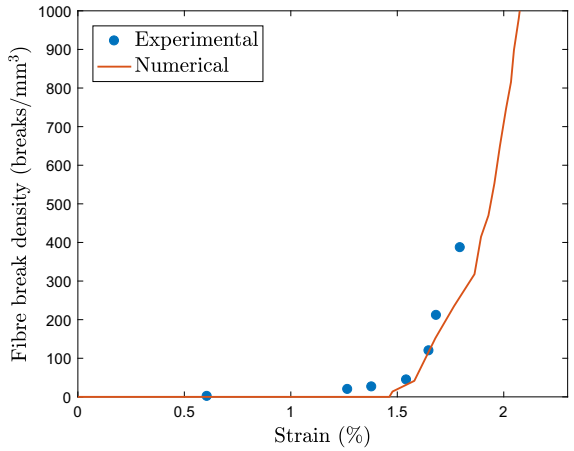

Fig. 13 Fibre break density in the fracture process: experimental and numerical results for unimodal Weibull distribution

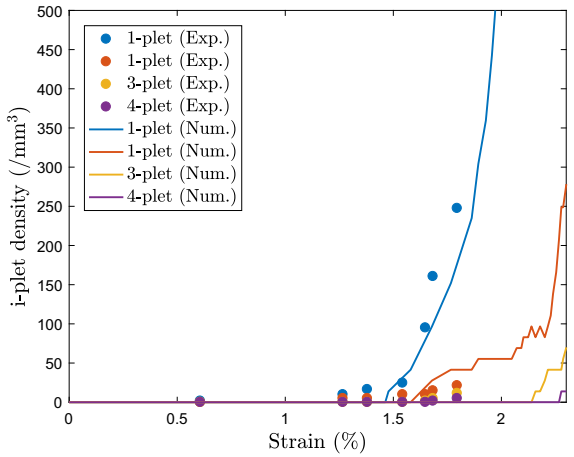

Fig. 14 i-plet growth during the fracture process as a function of the applied strain: experimental and numerical results for unimodal Weibull distribution

Regarding cluster formation (Fig. 14), the results show a better agreement with the experimental results, being the single fibre breaks (1-plet) well predicted, however, there is still an underestimation of the formation of clusters of broken fibres, that only occur for higher applied strains, which causes the failure to occur at higher strains. The reasons for these underestimation of cluster formation have already been mentioned and remain valid for the present case.

To better understand the fibre fracture process and the cluster formation, the fibre break density in each section of the RVE is plotted in Fig. 15. In this figure it is possible to see the stress-strain curve as well as the percentage of broken fibres in each section of the RVE

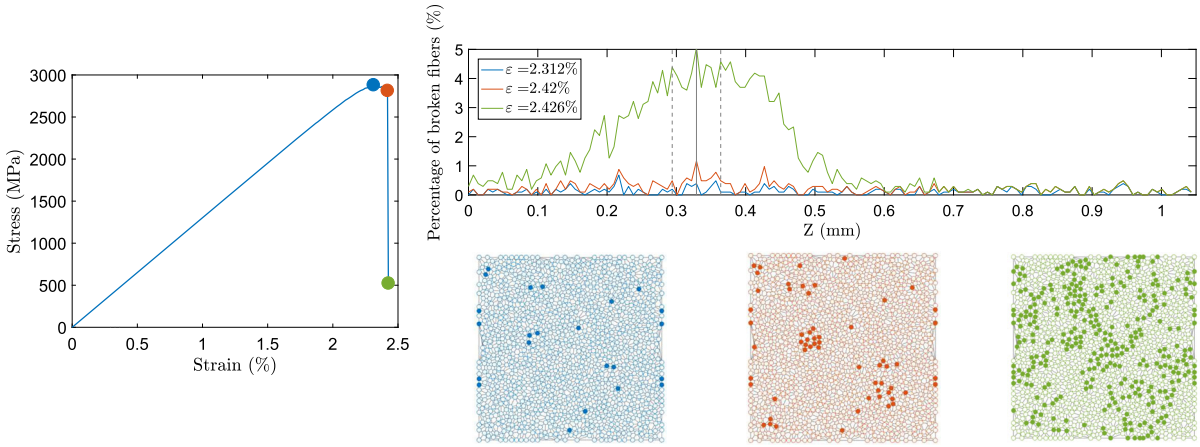

Fig. 15 Stress-strain curve of the T700 composite with a unimodal Weibull distribution, accompanied by the fibre break density in each section of the composite and the microstructures at the critical section at different stages

for all the sections along the fibre direction for three different applied strains, which are marked in the stress-strain curve. The microstructures shown represent the broken fibres within 10 fibre radius in each direction of the critical section, which was at $Z = 0.34$ mm. The critical section and the 10 fibre radius distance in each direction are plotted in the fibre break density image in full and dashed lines. In the microstructure in blue it is possible to see that there are a several broken fibres forming clusters, which grow with applied strain until the critical strain is achieved (figure in orange) leading to the failure of the material. After its failure (in green) it is possible to see that a large percentage of the fibres are broken and, therefore, the composite looses the load carrying capability.

3.5 Effect of fibre hybridization

The model proposed here can also be applied in the analysis of hybrid composites. It is expected that using more than one type of fibre will change the failure process and stress-strain behaviour of the material. If the hybridization is correctly designed it is possible to have a non-catastrophic failure of the material (Swolfs et al. 2014; Tavares et al. 2016). In this section the hybridization between the AS4 fibres, using the WOW distribution as in Sect. 3.2, with the M50S carbon fibres (Tanaka et al. 2014) whose properties are shown in Table 4 is analysed. To be able to use the WOW distribution for the M50S fibres, the value of α was chosen to be equal to the value of the AS4 fibre since no experimental data was available.

The fibre volume fraction considered in this section is 50%. Figure 16 shows a randomly generated microstructure of the AS4-M50S hybrid composite, where the AS4 fibres are shown in black and the M50S, which have a smaller radius, in grey. Figure 17 shows the stress-strain behaviour of both non-hybrid composites (AS4 and M50S) with the addition of a hybrid composite with 20% of M50S fibres and 80% of AS4 fibres.

It is shown that the M50S composite has an average strength of 1811 MPa, while the AS4 has an average strength of 1520 MPa. Due to the higher stiffness of the M50S fibres, the M50S composite has a lower failure strain than the AS4 one. The hybrid composite shows a behaviour very dissimilar from the non-hybrid ones, due to the fact that the hybridized fibres have different failure strains. This implies that when the M50S fibres (which are the lower elongation fibres) fail, the material does not fail due to the AS4 fibres that are still carrying load. This leads to the progressive failure seen in Fig. 17 in orange. The average strength of the hybrid compos-

Table 4 M50S carbon fibre properties (Tanaka et al. 2014)

R_f	2.65 μm
E_f	480 GPa
σ_0	4600 MPa
ρ	9
α	0.6

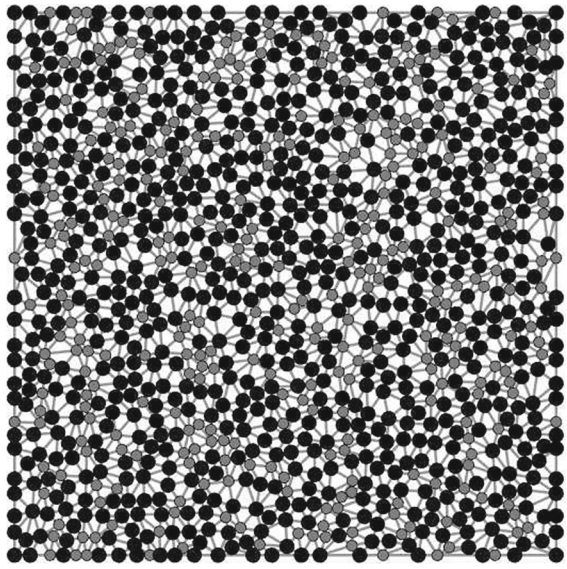

Fig. 16 Microstructure of a hybrid composite with 80% AS4 fibres and 20% M50S fibres

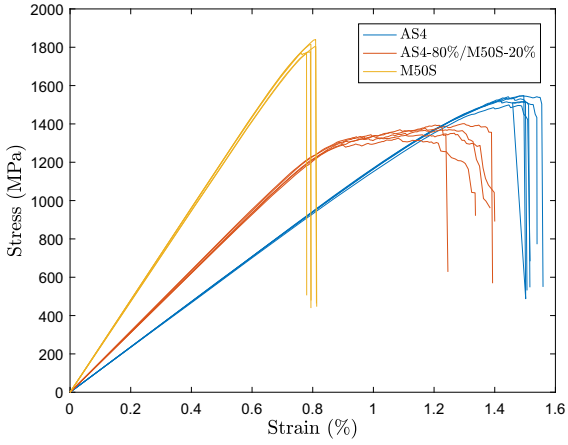

Fig. 17 Stress-strain behaviour of AS4 (in blue) and M50S (in Yellow) non-hybrid composites and AS4-M50S hybridization (in orange)

ite is 1344 MPa, with an failure strain of 1.22%. This is a reduction of both the strength and failure strain when compared with the AS4 composite, however, there is an increase in the stiffness of this material and the failure of the hybrid is non-catastrophic. A similar behaviour for this type of hybridization as been shown by Tavares et al. (2016) using different material models. Furthermore, Czél et al. (2017) has shown that it is possible to obtain non-catastrophic failure of hybrid composites using two different carbon fibres with different elastic and strength properties.

4 Conclusions

A spring element model that takes into account a random fibre packing was developed. The model is able to accurately capture the local stress fields surrounding a broken fibre, capturing the ineffective length of a broken fibre, as well as the stress concentrations in the intact fibres that surround a broken one. Unlike other models present in the literature, the stress redistribution resulting from a fibre break is not enforced and the corresponding stress concentrations in the surrounding fibres arise due to the solution of the global system of equations that governs the problem.

As a fibre dominated failure, the tensile failure of unidirectional composites largely depends on the accurate representation of the strength of the fibre elements. Several statistical distributions for fibre strength are available in the literature. To study their influence on the tensile behaviour of composites several simulations were performed using the traditional Weibull, the Power Law Accelerated Weibull and the Weibull of Weibulls strength distributions. The results were compared with the available experimental data and it was concluded that the Weibull of Weibulls fibre strength distribution leads to more accurate results in terms of the maximum stress. Nonetheless, it should be noted that size effects are present in composite materials and the simulated RVE and tested specimens used for comparison have different sizes.

As the matrix plays a large role in the stress transfer procedure, a study on the effect of matrix properties on the failure process was also analysed. The maximum shear strength has an influence on the UD strength and on the failure progression and cluster formation. The lower the interface strength is, the lower the failure strength of the composite and maximum cluster size are.

The fibre fracture and cluster development during the failure process was also analysed and compared with existing experimental results. It is concluded that similarly to other available models there was an overprediction of the single fibre breaks while underestimating the formation of clusters of larger sizes, specially planar clusters. This difference was attributed to the fact that the model does not consider the dynamic

effects present in the fracture process nor the effects of matrix cracking on the stress redistribution. Nevertheless, more insight on the cluster development and final fracture was obtained.

The developed model is also used to explore fibre hybridization. It is shown that the model is able to predict the non-catastrophic failure associated with hybrid composites. The usage of fibre hybrid composites promotes synergetic effects between the constituents that can lead to interesting material behaviours.

Acknowledgements The first author acknowledges the support of the Portuguese Government's Fundação para a Ciência e Tecnologia, under the Grant SFRH/BD/115872/2016. The second gratefully acknowledges the funding of Project NORTE-01-0145-FEDER-000022 SciTech Science and Technology for Competitive and Sustainable Industries, cofinanced by Programa Operacional Regional do Norte (NORTE2020), through Fundo Europeu de Desenvolvimento Regional (FEDER). The last author gratefully acknowledges the funding of Project PTDC/EMS-PRO/4732/2014, cofinanced by Programa Operacional Competitividade e Internacionalização and Programa Operacional Regional de Lisboa, through Fundo Europeu de Desenvolvimento Regional (FEDER) and by National Funds through FCT—Fundação para a Ciência e Tecnologia. The authors would like to thank the support of Dr. Stephane Mahdi, Dr. Christian Weimer and Christian Metzner (AIRBUS).

References

Argon AS (1974) Statistical aspects of fracture, chap 4. In: Broutman LJ (ed) Composite materials: fatigue and fracture, vol 5. Academic Press, New York, pp 153–190

Batdorf SB (1982) Tensile strength of unidirectionally reinforced composites—I. J Reinf Plast Compos 1(2):153–164. https://doi.org/10.1177/073168448200100206

Batdorf S, Ghaffarian R (1982) Tensile strength of unidirectionally reinforced composites—II. J Reinf Plast Compos 1(2):165–176. https://doi.org/10.1177/073168448200100207

Beyerlein IJ, Phoenix S (1996) Statistics for the strength and size effects of microcomposites with four carbon fibers in epoxy resin. Compos Sci Technol 56(1):75–92. https://doi.org/10.1016/0266-3538(95)00131-X

Cox HL (2002) The elasticity and strength of paper and other fibrous materials. Br J Appl Phys 3(3):72–79. https://doi.org/10.1088/0508-3443/3/3/302

Curtin WA (1991) Theory of mechanical properties of ceramic-matrix composites. J Am Ceram Soc 74(11):2837–2845. https://doi.org/10.1111/j.1151-2916.1991.tb06852.x

Curtin WA (2000) Tensile strength of fiber-reinforced composites: III. Beyond the traditional Weibull model for fiber strengths. J Compos Mater 34(15):1301–1332

Curtin WA, Takeda N (1998) Tensile strength of fiber-reinforced composites: I. Model and effects of local fiber geometry. J Compos Mater 32(22):2042–2059

Czél G, Jalalvand M, Wisnom MR, Czigány T (2017) Design and characterisation of high performance, pseudo-ductile all-carbon/epoxy unidirectional hybrid composites. Compos Part B Eng 111:348–356. https://doi.org/10.1016/j.compositesb.2016.11.049

DeJong MJ, Hendriks MA, Rots JG (2008) Sequentially linear analysis of fracture under non-proportional loading. Eng Fract Mech 75(18):5042–5056. https://doi.org/10.1016/j.engfracmech.2008.07.003

Delaunay B (1934) Sur la sphere vide. Izv Akad Nauk SSSR, Otdelenie Matematicheskii i Estestvennyka Nauk 7(793–800):1–2

Fukuda H (1985) Stress concentration factors in unidirectional composites with random fiber spacing. Compos Sci Technol 22(2):153–163. https://doi.org/10.1016/0266-3538(85)90082-X

Gulino R, Phoenix SL (1991) Weibull strength statistics for graphite fibres measured from the break progression in a model graphite/glass/epoxy microcomposite. J Mater Sci 26(11):3107–3118. https://doi.org/10.1007/BF01124848

Harlow DG, Phoenix SL (1978) The chain-of-bundles probability model for the strength of fibrous materials I: analysis and conjectures. J Compos Mater 12(2):195–214. https://doi.org/10.1177/002199837801200207

Hedgepeth JM, Dyke PV (1967) Local stress concentrations in imperfect filamentary composite materials. J Compos Mater 1(3):294–309. https://doi.org/10.1177/002199836700100305

Hedgepeth JM, Van Dyke P (1967) Local stress concentrations in imperfect filamentary composite materials. J Compos Mater 1(3):294–309. https://doi.org/10.1177/002199836700100305

Kelly A, Tyson W (1965) Tensile properties of fibre-reinforced metals: copper/tungsten and copper/molybdenum. J Mech Phys Solids 13(6):329–350. https://doi.org/10.1016/0022-5096(65)90035-9

Lamon J (2007) Mécanique de la rupture fragile et de l'endommagement: approches statistiques et probabilistes. Études en mécanique des matériaux et des structures, Hermes Science Publications. https://books.google.fr/books?id=VmihPQAACAAJ

Landis CM, McMeeking RM (1999) A shear-lag model for a broken fiber embedded in a composite with a ductile matrix. Compos Sci Technol 59(3):447–457. https://doi.org/10.1016/S0266-3538(98)00091-8

Madhukar MS, Drzal LT (1991) Fiber-matrix adhesion and its effect on composite mechanical properties: II. Longitudinal (0) and transverse (90) tensile and flexure behavior of graphite/epoxy composites. J Compos Mater 25(8):958–991. https://doi.org/10.1177/002199839102500802

Melro AR, Camanho PP, Pinho ST (2008) Generation of random distribution of fibres in long-fibre reinforced composites. Compos Sci Technol 68(9):2092–2102. https://doi.org/10.1016/j.compscitech.2008.03.013

Mishnaevsky L, Brøndsted P (2009) Micromechanisms of damage in unidirectional fiber reinforced composites: 3D computational analysis. Compos Sci Technol 69(7–8):1036–1044. https://doi.org/10.1016/j.compscitech.2009.01.022

Nishikawa M, Okabe T, Takeda N (2008) Determination of interface properties from experiments on the fragmentation pro-

cess in single-fiber composites. Mater Sci Eng A 480(1–2):549–557. https://doi.org/10.1016/j.msea.2007.07.067

Okabe T, Sekine H, Ishii K, Nishikawa M, Takeda N (2005) Numerical method for failure simulation of unidirectional fiber-reinforced composites with spring element model. Compos Sci Technol 65(6):921–933. https://doi.org/10.1016/j.compscitech.2004.10.030

Okabe T, Ishii K, Nishikawa M, Takeda N (2007) Prediction of tensile strength of unidirectional CFRP composites. J Jpn Soc Compos Mater 33(December 2014):205–212. https://doi.org/10.6089/jscm.33.205

Otero F, Oller S, Martinez X, Salomón O (2015) Numerical homogenization for composite materials analysis. Comparison with other micro mechanical formulations. Compos Struct 122:405–416. https://doi.org/10.1016/j.compstruct.2014.11.041

Padgett WJ, Durham SD, Mason AM (1995) Weibull analysis of the strength of carbon fibers using linear and power law models for the length effect. J Compos Mater 29(14):1873–1884

Pimenta S (2015) Fibre failure modelling, chap 25. In: Camanho PP, Hallet SR (eds) Numerical modelling of failure in advanced composite materials. Woodhead Publishing, Cambridge

Rots JG, Invernizzi S (2004) Regularized sequentially linear saw-tooth softening model. Int J Numer Anal Methods Geomech 28(78):821–856. https://doi.org/10.1002/nag.371

Scott A, Mavrogordato M, Wright P, Sinclair I, Spearing S (2011) In situ fibre fracture measurement in carbonepoxy laminates using high resolution computed tomography. Compos Sci Technol 71(12):1471–1477. https://doi.org/10.1016/j.compscitech.2011.06.004

Scott AE, Sinclair I, Spearing SM, Thionnet A, Bunsell AR (2012) Damage accumulation in a carbon/epoxy composite: comparison between a multiscale model and computed tomography experimental results. Compos Part A Appl Sci Manuf 43(9):1514–1522. https://doi.org/10.1016/j.compositesa.2012.03.011

Swolfs Y, Gorbatikh L, Romanov V, Orlova S, Lomov SV, Verpoest I (2013a) Stress concentrations in an impregnated fibre bundle with random fibre packing. Compos Sci Technol 74(0):113–120. https://doi.org/10.1016/j.compscitech.2012.10.013

Swolfs Y, Gorbatikh L, Verpoest I (2013b) Stress concentrations in hybrid unidirectional fibre-reinforced composites with random fibre packings. Compos Sci Technol 85:10–16. https://doi.org/10.1016/j.compscitech.2013.05.013

Swolfs Y, Gorbatikh L, Verpoest I (2014) Fibre hybridisation in polymer composites: a review. Compos Part A Appl Sci Manuf 67(0):181–200. https://doi.org/10.1016/j.compositesa.2014.08.027

Swolfs Y, McMeeking RM, Verpoest I, Gorbatikh L (2015a) Matrix cracks around fibre breaks and their effect on stress redistribution and failure development in unidirectional composites. Compos Sci Technol 108(0):16–22. https://doi.org/10.1016/j.compscitech.2015.01.002

Swolfs Y, Morton H, Scott A, Gorbatikh L, Reed P, Sinclair I, Spearing S, Verpoest I (2015b) Synchrotron radiation computed tomography for experimental validation of a tensile strength model for unidirectional fibre-reinforced composites. Compos Part A Appl Sci Manuf 77:106–113. https://doi.org/10.1016/j.compositesa.2015.06.018

Tanaka F, Okabe T, Okuda H, Kinloch IA, Young RJ (2014) Factors controlling the strength of carbon fibres in tension. Compos Part A Appl Sci Manuf 57(0):88–94. https://doi.org/10.1016/j.compositesa.2013.11.007

Tavares RP, Melro AR, Bessa MA, Turon A, Liu WK, Camanho PP (2016) Mechanics of hybrid polymer composites: analytical and computational study. Comput Mech 57(3):405–421. https://doi.org/10.1007/s00466-015-1252-0

Thionnet A, Chou HY, Bunsell A (2014) Fibre break processes in unidirectional composites. Compos Part A Appl Sci Manuf 65(0):148–160. https://doi.org/10.1016/j.compositesa.2014.06.009

Toyama N, Takatsubo J (2004) An investigation of non-linear elastic behavior of CFRP laminates and strain measurement using Lamb waves. Compos Sci Technol 64(16):2509–2516. https://doi.org/10.1016/j.compscitech.2004.05.007

Watanabe J, Tanaka F, Okuda H, Okabe T (2014) Tensile strength distribution of carbon fibers at short gauge lengths. Adv Compos Mater 23(5–6):535–550. https://doi.org/10.1080/09243046.2014.915120

Watson AS, Smith RL (1985) An examination of statistical theories for fibrous materials in the light of experimental data. J Mater Sci 20(9):3260–3270. https://doi.org/10.1007/BF00545193

Weibull W (1951) A statistical distribution function of wide applicability. J Appl Mech Trans ASME 58(7):1001–1010

Xia ZH, Curtin WA (2001) Multiscale modeling of damage and failure in aluminum-matrix composites. Compos Sci Technol 61(15):2247–2257. https://doi.org/10.1016/S0266-3538(01)00119-1

Xing J, Liu XR, Chou TW (1985) Dynamic stress concentration factors in unidirectional composites. J Compos Mater 19(3):269–275. https://doi.org/10.1177/002199838501900305

Zweben C (1968) Tensile failure of fiber composites. AIAA J 6(68):2325–2331. https://doi.org/10.2514/3.4990